2010 IEEE International Conference on Robotics and Automation
Anchorage Convention District
May 3-8, 2010, Anchorage, Alaska, USA

Towards Automated Self-Calibration of Robot Skin

Giorgio Cannata, Simone Denei, and Fulvio Mastrogiovanni

Abstract— **This paper deals with the problem of calibrating a large number of tactile elements (i.e., *taxels*) organized in a skin sensor system after fixing them to a robot body part. This problem has not received much attention in literature because of the lack of large-scale skin sensor systems. The proposed approach is based on a controlled compliance motion with respect to external objects whose pose is known, which allows a robot to determine the location of its own taxels. The major contribution of this work is the formulation of the skin calibration problem as a maximum-likelihood mapping problem in a 6D space, where both the position and the orientation of each taxel are recovered. An effective calibration process is envisaged that, given a compliance control law that assures prolonged contact maintainance between a given body part and an external object, returns a maximum-likelihood estimate of detected taxel poses. Simulations validate the approach.**

I. Introduction

During the past three decades, much effort has been devoted to the problem of providing robots with tactile skills [13], specifically in the context of grasping control [17], [9], [3], [2] and for enforcing safe interaction between robots and humans in unstructured environments [15], [18], [6].

In spite of the huge amount of research work devoted to the design of *tactile sensors*, a principled discussion about the actual large-scale development and effective deployment of a whole *skin sensor* system (i.e., covering large surfaces of body parts, and not small ones such as, e.g., fingertips) has not been fully addressed in literature. Experience suggests that developing skin sensor systems as networks of scalable and modular taxels conforming to robot body parts is only the first step [14]. Several issues have dramatic impact over system design when considering skin sensors in a global perspective: sensor calibration procedures, fault-tolerance [21], wiring, and massively distributed data processing, just to name a few.

A skin sensor system for humanoid robots taking scalability into account has been proposed in [10], where a network of taxels can be applied to arbitrarily curved surfaces. In spite of the low spatial resolution and high power consumption, the major contribution of [10] is twofold: (i) basic requirements for skin sensor systems are pointed out; (ii) the proposed solution allows a simple mechanical integration of transducers over curved surfaces. A similar approach to the design of integrated skin sensors has been proposed in [19], which allows to reach a higher spatial resolution at the price of a more limited capability in conforming to sharp curvatures. This problem has been addressed in [6], where a skin sensor system is described that can be bent to a very sharp curvature without being damaged. Conformability for multiple curvatures has been addressed in [16], where a triangular-based shape is adopted to ensure good conformal properties. Finally, an initial integration between whole body tactile information and motion control has been attempted in [11], where objects are pushed through body contact by means of tactile feeback.

Although the referenced work presents skin sensors at a system level, the arising issues are not addressed in depth. This paper is focused on the problem of *automated skin calibration*. This can be defined as *the automated process of finding the location of each taxel with respect to a known reference frame, after the skin sensor has been actually fixed on a robot body part*. Knowing taxels location is fundamental to develop more complex cognitive behaviors, such as quick response to sudden stimuli or compliant human-robot contacts. Specifying *by hand* the location of each taxel is not feasible, given the high number of sensors to calibrate and the periodic drift in their location due to mechanical effects caused by robot's activity.

The major contribution of this paper is a generic formulation of the skin calibration problem. In particular, an effective process is introduced allowing a robot to calibrate its own skin by means of purposively touching an object whose location is known, thereby activating taxels in a controlled way. The proposed method assumes the availability of: (i) a compliance control law that maintains the contact between the robot's body and an external object; (ii) force measurements to characterize the contact; (iii) a simple model of the contact mechanics. The paper is organized as follows: Section II details the proposed approach, formalizing calibration as a maximum-likelihood mapping problem, describing the adopted compliance control law and discussing the adopted force-based measurement model; Section III presents simulations to validate the overall approach; Conclusions follow.

II. Automated Calibration of Skin Sensors

In the following sections, the automated calibration problem is first formalized as a maximum-likelihood mapping problem in a 6D space. Each taxel is associated with a local reference frame, and therefore both position and orientation are considered. Then, a control architecture able to generate all the needed information is envisaged. As it can be noticed in Figure 1, tactile sensors are *transducers* that, when *stimulated* by an external force, notify both their *id* i and the measured pressure value p_i proportional to the contact force, according to the model described in [16],

All the authors are with the Department of Communication, Computer and System Sciences, University of Genova, Via Opera Pia 13, 16145, Genova, Italy. {name.surname}@unige.it.

This work has been partly supported by EC under contract number FP7-231500-RoboSKIN.

where a capacitance-based sensor has been discussed. To be localized, a taxel must be activated using a stimulus sufficient to trigger a response in the corresponding transducer. Taking advantage of the robot movement capabilities, the key idea is *to produce the required tactile stimuli by assigning the robot with a motion control law able to guarantee contact with an external object whose pose is known.*

A. A Maximum-Likelihood Formulation of Skin Calibration

Skin calibration is modelled as a maximum-likelihood mapping problem, which retrieves an estimated pose of taxels by minimizing a properly defined functional. Following a widespread approach to mapping problems [20], [1], the skin sensor is modelled using a graph structure, where *nodes* represent poses of taxels in terms of translation and rotation with respect to a common reference frame, and *edges* encode information about the relative displacement of two nearby taxels based on measurements. Specifically: $\mathbf{t}$ is a vector $(\mathbf{t}_1,...,\mathbf{t}_n)^T$ representing the 6D estimated poses $\mathbf{t}_i$ of all the n taxels to calibrate, i.e., a *configuration*; δ_{ji} describes a measured displacement between poses $\mathbf{t}_i$ and $\mathbf{t}_j$ (i.e., it refers to an actual observation of taxel j with respect to taxel i); Ω_{ji} is the *information* matrix modelling the likelihood associated with the measurement δ_{ji}; $h_{ji}(\mathbf{t})$ is the measurement model that computes an ideal observation of δ_{ji} using the current estimate of $\mathbf{t}$.

The goal is to find the taxels configuration $\mathbf{t}^*$ maximizing the likelihood of observations δ_{ji}, properly weighted by the corresponding Ω_{ji}, which is equivalent to minimizing the error associated with each displacement $e_{ji} = h_{ji}(\mathbf{t}) - \delta_{ji}$. Assuming that observations are characterized by a Gaussian error, the negative log-likelihood of an observation h_{ji} is given by:

$$H_{ji}(\mathbf{t}) = \frac{1}{2}\left(h_{ji}(\mathbf{t}) - \delta_{ji}\right)^T \Omega_{ji}\left(h_{ji}(\mathbf{t}) - \delta_{ji}\right) \propto e_{ji}(\mathbf{t})^T \Omega_{ji} e_{ji}(\mathbf{t}).$$

If observations are pairwise independent, the negative log-likelihood of the configuration $\mathbf{t}$ is

$$H(\mathbf{t}) = \frac{1}{2}\sum_{\langle j,i\rangle \in \Delta} e_{ji}(\mathbf{t})^T \Omega_{ji}(\mathbf{t}) e_{ji}(\mathbf{t}),$$

where Δ is the set of coupled indices for which an observation δ_{ji} has been acquired. The goal configuration $\mathbf{t}^*$ can be found by minimizing $H(\mathbf{t})$, i.e.,

$$\mathbf{t}^* = \arg\min_{\mathbf{t}} H(\mathbf{t}) \tag{1}$$

In literature, although this formulation is characterized by potential local minima, many algorithms exist to efficiently solve this problem, either exactly or with approximations [1], [20], [7], even on-line [8]. The adopted approach is very similar to what has been presented in [7].

B. A Compliance Motion Control Law for Skin Calibration

In order to generate measurements δ_{ji} and to solve Equation 1, a simulation scenario has been developed (see Figure 1), where the compliance control motion law has been implemented. At this stage, our aim is not to provide novel solutions to impedance control, rather to have a working environment where to test solutions for skin calibration. The envisaged motion control law is applied to a robotic arm on which end effector a spherical body S_e (of center location $\mathbf{x}_e$ and *nominal* radius r_0) has been installed that is covered by a skin sensor system. The goal is to vary in a controlled way the contact point $\mathbf{x}_c$ between S_e and another smaller sphere S_b whose center location $\mathbf{x}_b$ and radius $r_b \ll r_0$ are known. The relative movement between S_e and S_b is aimed at activating in sequence taxels located over the surface of S_e, registering their poses $\mathbf{t}_i$ and displacements δ_{ji} with respect to previously activated taxels $\mathbf{t}_j$. In principle, three requirements must be fulfilled by the control law: (i) it must guarantee that the contact between S_e and S_b is first established, and then maintained; (ii) the contact point $\mathbf{x}_c$ must vary in order to activate the largest number of taxels as possible: this is needed to add the more information as possible to the functional H_{ji}, given its *information* nature; (iii) the force originated by the interaction between S_e and S_b must be detected and controlled.

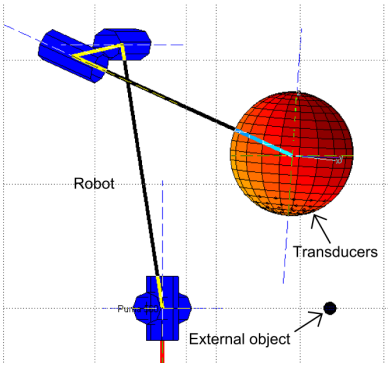

Fig. 1. The simulation environment: the *red* sphere is the robot's end effector, where transducers have been placed; the smaller *black* sphere is an external object of known position.

However, the envisaged control law is based on the following assumptions: (i) the contact between S_e and S_b is *frictionless*; (ii) the distance between S_e and S_b can be computed; (iii) S_e can be deformed as the result of the contact with the *indenter* S_b. It is convenient to define $\mathbf{n}$ as the unit vector normal to the common tangent plane between S_e and S_b and directed outward of S_e at the contact point $\mathbf{x}_c$ (see Figure 2 on the right side), i.e., $\mathbf{n} = \mathbf{x}_b - \mathbf{x}_e / \|\mathbf{x}_b - \mathbf{x}_e\|$.

Therefore, the contact point $\mathbf{x}_c$ can be defined as $\mathbf{x}_c = \mathbf{x}_b - r_b\mathbf{n}$, whereas the *effective* distance r_e between the contact point $\mathbf{x}_c$ and $\mathbf{x}_e$ is given by (see Figure 2 on the left side) $r_e = \|\mathbf{x}_c - \mathbf{x}_e\| = \|(\mathbf{x}_b - \mathbf{x}_e) - r_b\mathbf{n}\|$. As it can be seen in Figure 2, $\mathbf{x}_c$ can be thought as the point over the surface of S_b at the minimum distance r_e from $\mathbf{x}_e$. Therefore, after the contact, it always holds that $r_e < r_0$: the quantity $|r_e - r_0|$ is a measure of the local deformation of S_e.

As usual, the robot dynamic model in the joint space can be described as:

$$A(\mathbf{q})\ddot{\mathbf{q}} + B(\mathbf{q}\dot{\mathbf{q}})\dot{\mathbf{q}} + C(\mathbf{q}) = \tau_c + J_L^T(\mathbf{q})\mathbf{f}_c, \tag{2}$$

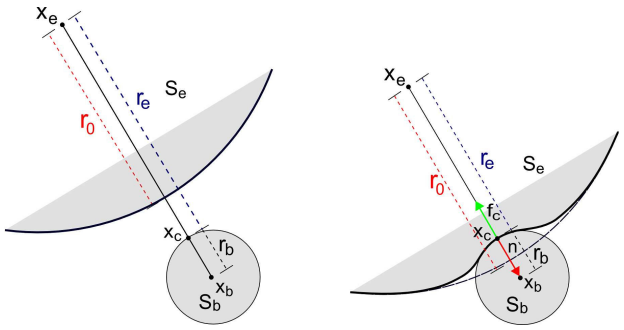

Fig. 2. Geometrical parameters. *Left*: before contact. *Right*: during contact.

where $A(\mathbf{q})$ is the *inertia* matrix, $B(\mathbf{q}\dot{\mathbf{q}})$ is the matrix of *centrifugal* and *Coriolis* effects, $C(\mathbf{q})$ is the matrix taking *gravitational* effects into account, τ_c are the *control joint torques*, whereas the terms $J_L^T(\mathbf{q})\mathbf{f}_c$ are torques exerted on the end effector.

According to considerations related to contact mechanics [5], the *normal* force vector $\mathbf{f}_c$ that can be reasonably imposed during contact regime can be expressed as:

$$\mathbf{f}_c = \begin{cases} -K_c\mathbf{n}(r_0 - r_e)^{\frac{3}{2}} & r_e < r_0 \\ 0 & r_e \geq r_0 \end{cases} \tag{3}$$

In particular, $\mathbf{f}_c$ as described in Equation 3 depends on a measure of the deformation $r_0 - r_e$ of S_e and is proportional to the gain K_c. The control torque can be imposed as

$$\tau_c = B(\mathbf{q},\dot{\mathbf{q}})\dot{\mathbf{q}} + C(\mathbf{q}) - L(\dot{\mathbf{q}} - \dot{\mathbf{q}}^*),$$

where $\dot{\mathbf{q}}^*$ is a reference vector for the joint velocities and L is a gain weighting the error $\dot{\mathbf{q}} - \dot{\mathbf{q}}^*$. The reference vector $\dot{\mathbf{q}}^*$ is the result of two different additive contributions, namely $\dot{\mathbf{q}}^* = \dot{\mathbf{q}}_f + \dot{\mathbf{q}}_r$, where $\dot{\mathbf{q}}_f$ is a velocity reference in the joint space that must be imposed to guarantee contact between S_e and S_b, whereas $\dot{\mathbf{q}}_r$ is a generic velocity reference that can be used to impose the contact point $\mathbf{x}_c$ to move on S_e. In order to express the vector $\dot{\mathbf{q}}^*$, we can consider the following Lyapunov function V:

$$V = \frac{1}{2}(\mathbf{f}_c - \mathbf{f}^*)^T(\mathbf{f}_c - \mathbf{f}^*) = \frac{1}{2}\partial\varphi^T\partial\varphi. \tag{4}$$

In Equation 4, $\mathbf{f}^*$ is the force vector reference that can be written as $\mathbf{f}^* = -f_{ref}\mathbf{n}$, where f_{ref} is the desired absolute value of the force to be applied to S_e along the contact normal $\mathbf{n}$. The Lyapunov function V in Equation 4 is by definition positive definite. Its derivative can be computed as:

$$\dot{V} = \partial\varphi\partial\dot{\varphi} = \partial\varphi\dot{\mathbf{f}}_c = (\mathbf{f}_c - \mathbf{f}^*)\dot{\mathbf{f}}_c.$$

Therefore, it is necessary to impose:

$$\dot{\mathbf{f}}_c = -\gamma\partial\varphi \tag{5}$$

where γ is a proportional gain. During contact, it is possible to compute the derivative of Equation 3, thereby obtaining:

$$\dot{\mathbf{f}}_c = -K_c\frac{d}{dt}\left[\mathbf{n}(r_0 - r_e)^{\frac{3}{2}}\right]. \tag{6}$$

Expanding the derivative in the right hand side of Equation 6, two additive terms are obtained:

$$\frac{d}{dt}\left[\mathbf{n}(r_0 - r_e)^{\frac{3}{2}}\right] = \frac{d\mathbf{n}}{dt}(r_0 - r_e)^{\frac{3}{2}} - \frac{3}{2}\mathbf{n}(r_0 - r_e)^{\frac{1}{2}}\frac{dr_e}{dt}, \tag{7}$$

where:

$$\frac{d\mathbf{n}}{dt} = -\frac{1}{\|\mathbf{x}_b - \mathbf{x}_e\|}\left(I - \mathbf{n}\mathbf{n}^T\right)\dot{\mathbf{x}}_e, \tag{8}$$

and

$$\frac{dr_e}{dt} = \mathbf{n}^T\left[\frac{r_b}{\|\mathbf{x}_b - \mathbf{x}_e\|}\left(I - \mathbf{n}\mathbf{n}^T\right) - I\right]\dot{\mathbf{x}}_e. \tag{9}$$

Substituting Equations 7, 8 and 9 into Equation 6, a relationship between $\dot{\mathbf{f}}_c$ and $\dot{\mathbf{q}}_f$ can be found as follows:

$$\begin{aligned}
\dot{\mathbf{f}}_c &= -K_c\frac{d}{dt}\left[\mathbf{n}(r_0 - r_e)^{\frac{3}{2}}\right] \\
&= -K_c\left\{-\frac{1}{\|\mathbf{x}_b - \mathbf{x}_e\|}\left(I - \mathbf{n}\mathbf{n}^T\right)(r_0 - r_e)^{\frac{3}{2}} + \right. \\
&\quad \left. -\frac{3}{2}(r_0 - r_e)^{\frac{1}{2}}\mathbf{n}\mathbf{n}^T\left[\frac{r_b}{\|\mathbf{x}_b - \mathbf{x}_e\|}\left(I - \mathbf{n}\mathbf{n}^T\right) - I\right]\right\}\dot{\mathbf{x}}_e \\
&= -K_c\underbrace{\left\{-\frac{(r_0 - r_e)}{\|\mathbf{x}_b - \mathbf{x}_e\|}\left(I - \mathbf{n}\mathbf{n}^T\right) + \frac{3}{2}(r_0 - r_e)^{\frac{1}{2}}\mathbf{n}\mathbf{n}^T\right\}}_{\zeta}\dot{\mathbf{x}}_e \\
&= -K_c\zeta\dot{\mathbf{x}}_e = -K_c\zeta J_L\dot{\mathbf{q}}_f.
\end{aligned} \tag{10}$$

Recalling Equation 5, Equation 10 can be rewritten as:

$$-K_c\zeta J_L\dot{\mathbf{q}}_f = -\gamma\partial\varphi,$$

which is a system of equations that can be solved using a simple least square method, thereby allowing to express $\dot{\mathbf{q}}_f$ as function of $\mathbf{f}_c$ and $\mathbf{f}^*$, as follows:

$$\dot{\mathbf{q}}_f = \frac{\gamma}{K_c}(\zeta J_L)^+\partial\varphi = \frac{\gamma}{K_c}(\zeta J_L)^+(\mathbf{f}_c - \mathbf{f}^*). \tag{11}$$

Equation 11 guarantees that S_e reaches and keeps contact with S_b at the desired force reference $\mathbf{f}^*$. As soon as the relative movement between S_e and S_b occurs, taxels on the surface of S_e are sequentially activated. Since many taxels at once are activated as long as the contact point $\mathbf{x}_c$ moves on the surface of S_e, a model of the contact mechanics and a measurement model h_{ji} must be designed to retrieve the pose of each taxel and their displacements with respect to nearby taxels.

C. A Measurement Model for Automated Skin Calibration

In order to solve Equation 1, a model is needed relating the contact point $\mathbf{x}_c$, the exerted force $\mathbf{f}_c$, the pressure measurements p_i reported by taxels and taxel poses $\mathbf{t}_i$ with respect to a given reference frame. Since the normal force that is exerted by the indenter S_b entails a pressure distribution over a small portion of the surface of S_e, a single contact point $\mathbf{x}_c$ causes many taxels to be activated at the same time: both their poses $\mathbf{t}_i$ and pairwise mutual displacements δ_{ji} with respect to nearby taxels of pose $\mathbf{t}_j$ must be computed to carry out the calibration process. A model for determining the pressure distribution given the contact point $\mathbf{x}_c$ and the exerted force $\mathbf{f}_c$ is required to correctly estimate the pose

of activated taxels. In this work, we simply refer to the seminal Hertz contact model, whose properties have been exhaustively validated in literature [12], [5]. In particular, the Hertz model accounts for the relationship between the normal force $\mathbf{f}_c$ and the normal deflection at the contact interface in the case of two elastic spheres. The Hertz model is usually characterized by a number of assumptions[1]: however, the model proves to be robust against assumptions relaxation.

According to the Hertz model, when the two bodies S_e and S_b are subject to a normal force $\mathbf{f}_c$, each body undergoes a *local* contact surface deflection. The Hertz model predicts that the contact surface is *flat*, *circular* of radius r_a and *centered* around $\mathbf{x}_c$. In particular, the pressure distribution $\mathscr{P}(r_p)$ over the contact area can be computed as:

$$\mathscr{P}(r_p) = p_{\mathbf{x}_c}\left(1 - \frac{r_p^2}{r_a^2}\right)^{\frac{1}{2}}. \tag{12}$$

In Equation 12, r_p is the radial *distance* from the center of the contact area $\mathbf{x}_c$ in the outward direction, whereas $p_{\mathbf{x}_c}$ is the peak of the pressure distribution occurring at $\mathbf{x}_c$. Both $p_{\mathbf{x}_c}$ and r_a are unknown. The peak can be easily computed as follows:

$$p_{\mathbf{x}_c} = \frac{3f_c}{2\pi r_a^2}, \tag{13}$$

whereas the radius of the contact area r_a is given by:

$$r_a = \left(\frac{3f_c\mathscr{R}}{4\mathscr{E}}\right)^{\frac{1}{3}}. \tag{14}$$

The radius of the contact area depends on two quantities: $\mathscr{E}$ is a constant taking the *elastic* properties of the materials of both S_e and S_b into account, while $\mathscr{R}$ is the *effective* curvature radius of the two bodies in contact [12], [5].

Assuming that taxel activation follows the Hertz model in Equation 12, and knowing both the position $\mathbf{x}_c$ and the exerted force $\mathbf{f}_c$ over the contact point, it is possible to compute the distance r_i of an activated taxel of pose $\mathbf{t}_i$ measuring a pressure p_i as:

$$r_i = r_a\sqrt{1 - \left(\frac{p_i}{p_{\mathbf{x}_c}}\right)^2}. \tag{15}$$

Equation 15 provides an estimate of an activated taxel distance r_i from the current position of the contact point $\mathbf{x}_c$ on the basis of the taxel response p_i. Since, from Equation 15, only distance measurements are available, one possibility is to use a *trilateration* method to determine the exact geometrical pose $\mathbf{t}_i$ of the taxel. Trilateration allows to determine the exact location $\mathbf{t}_i$ of a detected taxel if three subsequent distance measurements $r_{i,1}$, $r_{i,2}$ and $r_{i,3}$ of the same taxel (taken with respect to three different contact points $\mathbf{x}_{c,1}$, $\mathbf{x}_{c,2}$ and $\mathbf{x}_{c,3}$) are considered. However, in order to apply trilateration, three assumptions must be satisfied:

[1]A discussion about the assumptions underlying the Hertz model is out of the scope of the paper: the interested reader is referred to [5]. Current work is carried out to determine a more detailed model based on a real prototype of skin sensor systems.

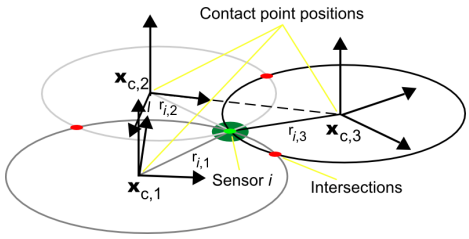

Fig. 3. The trilateration process.

(i) the contact model in Equation 12 *correctly* describes forces exerted over S_e; (ii) the three contact positions $\mathbf{x}_{c,1}$, $\mathbf{x}_{c,2}$ and $\mathbf{x}_{c,3}$ from where distance measurements are taken must be sufficiently close to each other to consider *flat* the surrounding surface, which is akin to what is stated by the Hertz model; (iii) the three contact positions must not be perfectly aligned, which is reasonable for realistic body parts.

The trilateration process is described using a constructive example (see Figure 3). At a given time instant, S_e and S_b are assumed to be in contact in $\mathbf{x}_{c,1}$. For simplicity, only one taxel of unknown pose $\mathbf{t}_i$ is assumed to be active during the whole process with a pressure measurement p_i. Since the normal force $\mathbf{f}_{c,1}$ at the contact point is assumed to be measurable, the peak pressure $p_{\mathbf{x}_{c,1}}$ can be computed using Equation 13. At the same time, the radius $r_{a,1}$ of the contact area can be determined using Equation 14. As a consequence, recalling Equation 15, the distance $r_{i,1}$ between the contact point $\mathbf{x}_{c,1}$ and the active taxel can be computed as follows:

$$r_{i,1} = r_{a,1}\sqrt{1 - \left(\frac{p_i}{p_{\mathbf{x}_{c,1}}}\right)^2}.$$

As it can be seen in Figure 3, $r_{i,1}$ identifies a circle centered in $\mathbf{x}_{c,1}$. The unknown pose $\mathbf{t}_i$ lies on this circle. At a subsequent time instant, the compliance motion control law causes the contact point to move in $\mathbf{x}_{c,2}$. Again, given the normal force $\mathbf{f}_{c,2}$, it is possible to compute the peak pressure $p_{\mathbf{x}_{c,2}}$ and the radius $r_{a,2}$, thereby obtaining a new distance measurement $r_{i,2}$. This identifies a second circle centered in $\mathbf{x}_{c,2}$. The pose $\mathbf{t}_i$ must lie on the intersection between the two circles. However, in the general case, the two circumferences intersect into two distinct points: as a matter of fact, a third distance measurement is required. When $r_{i,3}$ is available, $\mathbf{t}_i$ can be easily found.

Trilateration constitutes the measurement model $h_{ji}(\mathbf{t})$ introduced in Section II-A. When several taxels are active at the same time, once their poses are retrieved by trilateration, it is straightforward to compute mutual displacements δ_{ji}. Finally, it is worth noticing that uncertainties Ω_{ji} associated with displacements are assumed to be Gaussian, which is reasonable given the assumptions underlying both the Hertz model and the trilateration process[2]. At this point, all the data needed to solve Equation 1 are available.

[2]Experiments aimed at better characterizing the measurement errors are in the upcoming research agenda.

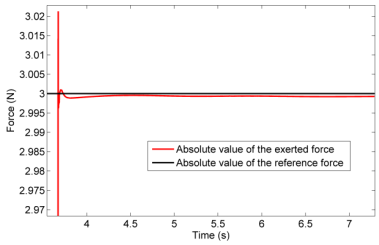

Fig. 4. Imposed *versus* reference normal force.

III. Experimental Validation

The calibration process has been validated in a simulated scenario. The end effector of an anthropomorphic arm, a spherical body S_e (in *red* in Figure 1), is provided with a skin sensor system. Taxels can be activated by the physical interaction with a small sphere S_b (in *black* in Figure 1) whose pose is known. The interaction is managed using the compliance motion control law described in Section II-B. As long as the simulation runs, the pose of the contact point and sensor pressure measurements are registered. After the simulation phase, the minimization described in Equation 1 is performed, thereby recovering the maximum-likelihood estimate of the taxels.

The simulation environment is implemented using the well-known Robotics Toolbox [4]. S_e is a sphere of radius $0.1m$ whose material is *elastic* and *deformable*. In the bottom part of the sphere 80 taxels are located at a mean distance of $5mm$. Taxels are modelled as *ideal transducers* of $2mm$ radius that can measure the exact exerted force according to the model described in [16]: the pressure $p_{\mathbf{x}_c}$ is assumed to be uniformly distributed over the single taxel area. Differently from the sphere mounted on the robot's end effector, S_b is not deformable and its radius is sensibly shorter, i.e., $0.01m$.

An example of the force $\mathbf{f}_c$ exerted by S_b over S_e is shown in Figure 4. After the initial impact assessment, the exerted force converges towards the reference value $\mathbf{f}^* = 3N$, thereby guaranteeing the compliance between the two spheres while relative motion is achieved. During this phase, taxel distances from the contact point are retrieved by trilateration, thereby recovering an initial guess of taxel locations $\mathbf{t}_i$ and therefore measurements δ_{ji}. Figure 5 shows a maximum-likelihood estimate of taxel poses from a bottom-up perspective assuming ideal pose measurements as a result of trilateration.

In real-world scenarios, measurements are uncertain since: (i) the contact model only approximates the real behavior of the skin sensor; (ii) different transducer responses may differ from each other. Therefore, a Gaussian error is introduced around the pose estimated by trilateration. Figures 6, 7 and 8 show an example of the minimization process when the original measurements are perturbated by $\mathcal{N}(0m, 1mm^2)$, respectively after 1, 100 and 1000 iterations.

Figure 6 shows the first iteration of the minimization algorithm. Since only the displacements δ_{ji} are actually optimized, all the sensors are initially located in $O = (0,0,0)^T$. Figure 7 shows the estimate after 100 iterations: major improvements are made with respect to the initial configuration. However, as it can be noticed in Figure 8, subsequent iterations only allow minor improvements on the final estimate.

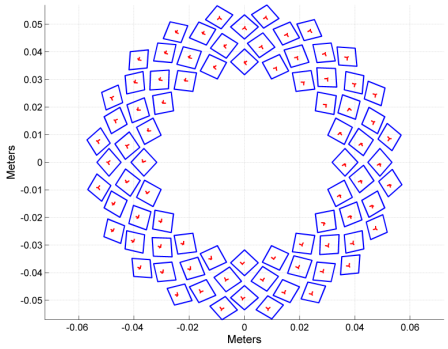

Fig. 5. Maximum-likelihood estimation of taxels (in *blue*) from ideal measurements: estimated local reference frames are depicted in *red*.

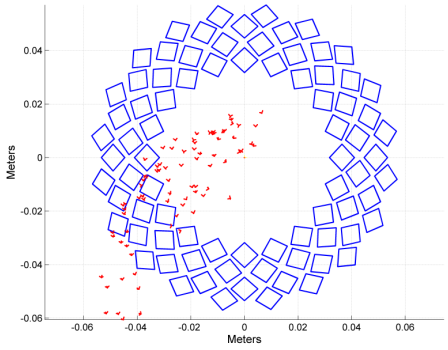

Fig. 6. Maximum-likelihood estimate of taxels after 1 iteration.

Simulations are used in the design process of real system prototypes (see Figure 9). We performed experiments to characterize the required mean initial estimate resulting from the trilateration process given the improvements obtained using calibration: when the initial error is less than $3mm$, improvements due to the optimization are around 20%. With an initial error between 3 and $6mm$, improvements are up to 50%, whereas for higher initial mean errors they are less significant.

IV. Conclusions

This paper deals with the calibration of a skin sensor system covering large parts of robots. The major paper contribution is the formulation of the problem in terms of maximum-likelihood mapping: the pose of each taxel composing the skin sensor can retrieved by minimizing a functional that considers mutual displacements between taxels as well as the associated uncertainty. A simulation test-bed has been used for validation: the end effector of an

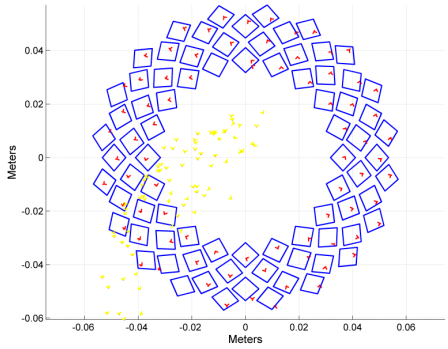

Fig. 7. Maximum-likelihood estimate of taxels after 100 iterations: the previous estimate is depicted in *yellow*.

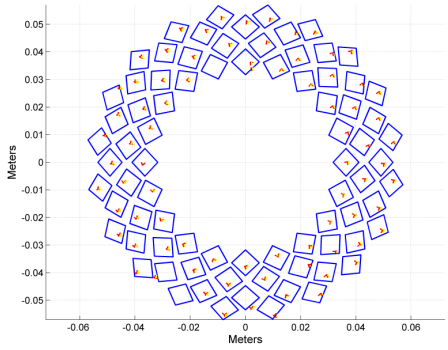

Fig. 8. Maximum-likelihood estimate of taxels after 1000 iterations.

anthropomorphic arm is provided with a sensorized sphere, and controlled through a compliance motion law in order to guarantee the activation of taxels by means of contact with an external object. In spite of the many simplifying assumptions, results show that the described calibration process is feasible, and provide also guidelines for the performance required to the motion control law. Implementation on a real set-up, as well as an extention to self-touching (e.g., two arms *rubbing* around each other) are subject of current work.

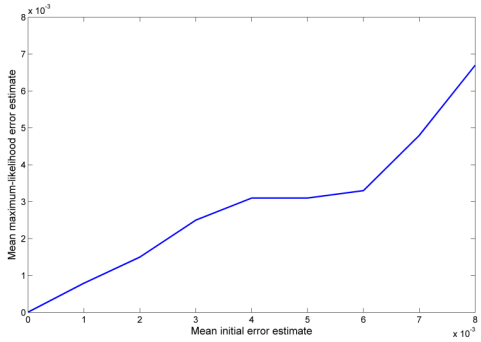

Fig. 9. Mean initial estimate *versus* mean maximum-likelihood errors.

REFERENCES

[1] W. Burgard, C. Stachniss, G. Grisetti, B. Steder, R. Kuemmerle, C. Dornhege, M. Ruhnke, A. Kleiner, J.D. Tardos. A Comparison of SLAM Algorithms Based on a Graph of Relations. In *Proc. of the 2009 IEEE/RSJ Int.l Conf. on Intelligent Robots and Systems (IROS'09)*, St. Louis, MO, October 11–15, 2009.

[2] J.J. Cabibihan, B.B. Edin, L. Beccai and M.C. Carrozza. A Bio-inspired Approach for the Design and Characterization of a Tactile Sensory System for a Cybernetic Prosthetic Hand. In *Proc. of the 2006 IEEE Int.l Conf. on Robotics and Automation (ICRA'06)*, Orlando, FL, May 15–19, 2006.

[3] G. Cannata and M. Maggiali. An Embedded Tactile and Force Sensor for Robotic Manipulation and Grasping. In *Proc. of the 2005 IEEE-RAS Int.l Conf. on Humanoid Robots (Humanoids 2005)*, Tsukuba, Japan, December 5–7, 2005.

[4] P.I. Corke. MATLAB Toolboxes: Robotics and Vision for Students and Teachers. In *IEEE Robotics and Automation Magazine*, vol. **14**(4):16–17, December 2007.

[5] E. Dintwa, E. Tijskens1 and H. Ramon. On the Accuracy of the Hertz Model to Describe the Normal Contact of Soft Elastic Spheres. In *Granular Matter*, vol. **10**(3):209–221, March 2008.

[6] V. Duchaine, N. Lauzier, M. Baril, M.A. Lacasse and C. Gosselin. A Flexible Robot Skin for Safe Physical Human Robot Interaction. In *Proc. of the 2009 IEEE Int.l Conf. on Robotics and Automation (ICRA'09)*, Kobe, Japan, May 12–17, 2009.

[7] G. Grisetti, S. Grzonka, C. Stachniss, P. Pfaff and W. Burgard. Efficient Estimation of Accurate Maximum Likelihood Maps in 3D. In *Proc. of the 2007 IEEE/RSJ Int.l Conf. on Intelligent Systems and Robots (IROS'07)*, San Diego, CA, October 2007.

[8] G. Grisetti, D. Lodi Rizzini, C. Stachniss, E. Olson and W. Burgard. Online Constraint Network Optimization for Efficient Maximum Likelihood Mapping. In *Proc. of the 2008 IEEE Int.l Conf. on Robotics and Automation (ICRA'08)*, Pasadena, CA, May 2008.

[9] T. Komatsu, H. Kawasaki, T. Komatsu and K. Uchiyama. Dexterous Anthropomorphic Robot Hand with Distributed Tactile Sensor: Gifu Hand II. In *IEEE Trans. on Mechatronics*, vol. **7**(3):296–303, 2002.

[10] Y. Kuniyoshi, Y. Ohmura and A. Nagakubo. Conformable and Scalable Tactile Sensor Skin for Curved Surfaces. In *Proc. of the 2006 IEEE Int.l Conf. on Robotics and Automation (ICRA'06)*, Orlando, FL, May 15–19, 2006.

[11] Y. Kuniyoshi and Y. Ohmura. Humanoid Robot which can Lift a 30kg Box by Whole Body Contact and Tactile Feedback. In *Proc. of the 2007 IEEE/RSJ Int.l Conf. on Intelligent Robots and Systems (IROS'07)*, San Diego, CA, September 29–October 2, 2007.

[12] K.L. Johnson. Contact Mechanics. Cambridge University Press, 1985.

[13] V.J. Lumelsky, M.S. Shur and S. Wagner. Sensitive Skin. World Scientific, 2000.

[14] V.J. Lumelsky, M.S. Shur and S. Wagner. Sensitive Skins: Electronics on Flexible Substrates. In *IEEE Sensors Journal*, vol. **1**(1):41–51, 2001.

[15] V.J. Lumelsky. Sensing, Intelligence, Motion: How Robots and Humans Move in an Unstructured World. Wiley-Interscience, 2005.

[16] M. Maggiali. Artificial Skin for Humanoid Robots. Ph.D. Disseration, University of Genova, 2008.

[17] P. Meusel, H. Liu and G.A. Hirzinger. A Tactile Sensing System for the Three-Finger Robot Hand. In *Proc. of the Fourth Int.l Symposium on Measurement and Control in Robotics (ISMCR'95)*, Smolenice Castle, Slovakia, June 12–16, 1995.

[18] T. Miyashita, T. Tajika and H. Ishiguro. Automatic Categorization of Haptic Interactions - What Are the Typical Haptic Interactions between a Human and a Robot? In *Proc. of 2006 IEEE-RAS Int.l Conf. on Humanoid Robots (Humanoids2006)*, Genova, Italy, December 4–6, 2006.

[19] T. Mukai, M. Onishi, T. Odashima, S. Hirano and Z. Luo. Development of the Tactile Sensor System of a Human-Interactive Robot RI-MAN. In *IEEE Trans. on Robotics*, vol. **24**(2):505–512, April 2008.

[20] S. Thrun, W. Burgard and D. Fox. Probabilistic Robotics. The MIT Press, 2005.

[21] D. Um and V.J Lumelsky. Fault-tolerance via Analytic Redundancy for a Modularized Sensitive Skin. In *Proc. of the 1999 IEEE/RSJ Int.l Conf. on Intelligent Robots and Systems (IROS'99)*, Kyongju, South Korea, October 13–17, 1999.